Renewable Energy 99 (2016) 996–1007

Contents lists available at ScienceDirect

Renewable Energy

journal homepage: www.elsevier.com/locate/renene

LPV-based active power control of wind turbines covering the complete wind speed range

Fernando A. Inthamoussou [a, b, *], Hernán De Battista [a, b], Ricardo J. Mantz [a, c]

[a] Instituto UNLP-CONICET LEICI, Facultad de Ingeniería, Universidad Nacional de La Plata, CC 91, 1900, La Plata, Argentina
[b] CONICET, Argentina
[c] CICpba, Argentina

ARTICLE INFO

Article history:
Received 17 February 2016
Received in revised form
2 June 2016
Accepted 25 July 2016
Available online 5 August 2016

Keywords:
Wind turbines
Control
LPV
Active power control

ABSTRACT

This paper focuses on the active power control of wind turbines. Modern grid codes increasingly demand active power control in order to guarantee utility grid stability under high wind energy penetration. Active power control provides capabilities to regulate wind power below rated, to maintain a power reserve, to indirectly regulate the grid frequency, etc. New controllers are necessary to tackle the extended operating modes and new objectives. This paper addresses the control problem using LPV techniques, since they are particularly suited to cope with the nonlinearities that arise along the extended operating region. The proposed controller was evaluated on a 5 MW wind turbine benchmark. For that purpose, very demanding and realistic testing scenarios were built using the FAST aeroelastic wind turbine simulator as well as standardized wind speed profiles. The proposed controller was compared with the gain scheduled PI traditionally used for wind turbine control and also with a gain scheduled $\mathscr{H}_\infty$ controller. Finally, a comparative load analysis is presented with the aim of showing that the softer and lower pitch activity of the proposed controller decreases the extreme load events.

1. Introduction

Nowadays, wind energy is the most competitive worldwide available renewable resource. The use of lighter materials, the construction of larger turbines and the incorporation of versatile automatic control strategies, among other factors, have dramatically reduced the wind energy costs during the past decades. Because of its huge potential, more and more wind energy is being integrated to the utility grids.

Historically, wind power plants have been operated to harness as much energy as possible. Because of the variability and uncertainty of the primary resource, wind power has been considered as a burden on the electric power system. As wind penetration rose, limited production at large power plants level according to TSO demands, resource forecasting and energy storage (mainly water pumping) have been increasingly exploited to partially mitigate these drawbacks. Today, wind power is supplying up to 20% of energy demand in some regions of the world, exceeding by far the predictions of some decades ago [1]. Naturally, with this penetration level, the technical regulations for wind power connection to the utility grid are becoming more demanding. In fact, wind power plants are being required to provide some ancillary services like some conventional power plants do, as well as to show grid fault ride through capabilities [2,3].

Currently, there is an increasing interest in equipping wind turbines with active power control (APC) [4–8]. APC allows wind farms to track the grid power demand by adjusting the power outputs of the wind turbines rather than starting up and shutting down some of them. This method introduces less perturbations to the grid, causes less stress to the wind turbines and is more powerful to provide grid support. Additionally, APC seems indispensable for wind turbine connection to a micro-grid, particularly during island mode.

APC requires operating the wind turbine on an extended region and a control system according to the new control strategy. The classical decentralized PI control of pitch and torque can still be used for APC with some few modifications regarding the reference computation and pitch controller tuning [5]. In particular, pitch PI controller is gain scheduled in industry in order to compensate for one of the system nonlinearities along the classical operating locus

* Corresponding author. Instituto UNLP-CONICET LEICI, Facultad de Ingeniería, Universidad Nacional de La Plata, CC 91, 1900, La Plata, Argentina.
E-mail address: intha@ing.unlp.edu.ar (F.A. Inthamoussou).

http://dx.doi.org/10.1016/j.renene.2016.07.064
0960-1481/

[9]. Obviously, the performance of this controller drops when it is applied on wind turbines with extended operating modes (as APC). Although the gain scheduling could be redesigned accordingly, the inherent structural constraint of PI control imposes severe limitations to the achievable performance on the extended operating region.

LPV allows a formal formulation of gain scheduling control design [10,11]. In addition, to accomplishing some guaranties of stability and performance, this theoretical approach simplifies considerably the control design. Furthermore, the tools to design LPV gain-scheduled controllers are similar to $\mathscr{H}_\infty$, thus being very intuitive and familiar to the control community. In previous works, LPV controllers have been developed for wind turbines where the operating locus, system model and controller are parameterized by a single scheduling variable [12–16]. Since these controllers are designed for operation along the conventional control locus, i.e. along the curve of maximum power capture up to rated power, they are not capable of regulating the active power. Preliminary results about gain scheduling design of APC for active-stall and variable-pitch wind turbines have been presented in Refs. [17] and [18], respectively. The latter proposes a multivariable LPV control of both pitch and torque valid only in the high wind speed region.

In this paper, we propose a novel LPV control design method for variable-pitch wind turbines with APC features. This method includes anti-windup (AW) compensation so that the controller can be applied over the complete wind speed range. The standard decoupled pitch and torque control structure is adopted here instead of the multivariable approach followed in Refs. [16,18], thus reducing the gap with the conventional control structure and the practical implementation. Furthermore, the LPV controller is parameterized by two known scheduling variables: pitch and power demand, so its implementation is easier than in previous approaches where the wind speed is a controller parameter [12,16].

The control proposal considers speed and power regulation along the whole wind speed envelope. This APC proposal is thought for both stand-alone and wind farm operation. In the case of stand-alone operation, the power set-point is determined and sent to the turbine by the grid operator. On the other hand, in the case the wind turbine integrates a wind farm, the power set-point is determined and sent to the turbine by the Wind Power Plant Controller. In the latter case, APC control of the wind turbines allows regulating the output plant power without shutting down and starting up some wind turbines as function of available and demanded power. Obviously, this mode reduces the turbine stress. The WPPC sends to the wind turbine their reactive power set-points also. Q regulation is carried out at power electronics converter. In our paper, we deal only with active power control, which can be decoupled from the Q control. In fact, the pitch dynamics is much slower than the power converter current dynamics. Wind turbines as large as this one is commonly found in wind farms, whereas much smaller wind turbines are common in stand-alone applications. Anyway, the proposed controller is equally valid for both applications.

The proposed control has been thoroughly evaluated by numerical simulation using the FAST (Fatigue, Aerodynamics, Structures, and Turbulence) code developed by the National Renewable Energy Laboratory (NREL) [19]. The controller performance has been assessed perturbing the wind turbine with very demanding wind speed profiles established in IEC standards.

2. Problem statement

To provide ancillary services such as frequency and voltage support, grid fault ride through and grid recovery support, wind turbines with active and reactive power control features are highly convenient. To some extent, active and reactive control are decoupled. Whereas APC is achieved by actuating on the pitch and torque commands, reactive power control is performed at the electronic converters. This paper focuses on the active power control, which is a much more challenging problem.

The typical control objective of wind turbines is to maximize the energy capture while operating the turbine within safety limits. Accordingly, the conventional operation modes of wind turbines are maximum power tracking at low wind speeds and regulation at the nominal point (rated power and speed) at high wind speeds.

The conventional control strategy is usually plotted on the torque – rotational speed plane although a more complete representation is achieved in the torque – rotational speed –pitch space (thick line in Fig. 1). Three regions can be identified along the operating locus:

- Region 1: in this region, the generator torque is varied in proportion to speed. Along the quadratic curve identified by the extreme points *A* and *B*, where the turbine is operated at optimum tip speed ratio (TSR) and optimum pitch, the power conversion is maximum. Along the line *B*–*C*, the turbine looses some efficiency as TSR is reduced with the purpose of reaching region 2 at an appropriate point. This line is sometimes called region $1\frac{1}{2}$.
- Region 2: in this region, either torque or power is kept constant while speed is below rated. It is usually called transition region, sometimes including region $1\frac{1}{2}$, between the maximum power tracking curve and the nominal point *N*. In Fig. 1, region 2 is the constant torque segment *C*–*N*.
- Region 3: in this high wind speed region, the blades are pitched to keep operation at the nominal point *N* where both power and speed are regulated at their rated values. When plotted on the torque – rotational speed – pitch space, region 3 is identified by the segment *N*–*M*.

2.1. Control strategy for active power control

APC enables new operation modes such as generation with reserve, generation with balance and gradient limitation [20]. Fig. 2 sketches them. Therefore, wind turbines with APC should be controlled to track the reference value whenever possible. That is, their control objective is to maximize the energy capture while operating the turbine within safety limits and without exceeding the reference power. Different control strategies can be applied to limit the power production below rated. Perhaps the most obvious one consists in operating the wind turbine below the conventional operating locus. Fig. 1 shows this control strategy and displays the operating curves for different power demands. Obviously, the different operating regions are extended or modified to achieve the new objective.

- Region 1e: this region is essentially the same as before, but transition to region 2 may occur before reaching point *C* since the power demand may be lower than the one corresponding to point *C*.
- Region 2e: this region is all the region below the curve *A*–*N* on the torque-speed plane. Once reached the power demand, the operating point moves along a constant–power hyperbola until reaching rated speed.
- Region 3e: this region is all the area below the line *N*–*M* on the torque-pitch plane. In this area, the blades are pitched to achieve the power demand at rated speed.

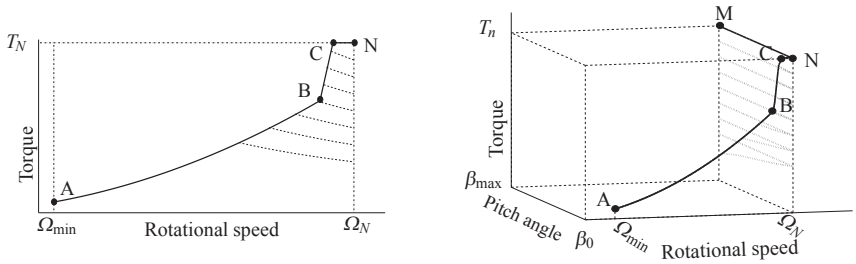

Fig. 1. Family of operating curves for a variable-speed variable-pitch wind turbine at different power demands (Thick trace: traditional operating locus). Right: 3D representation. Left: projection onto the torque – rotational speed plane.

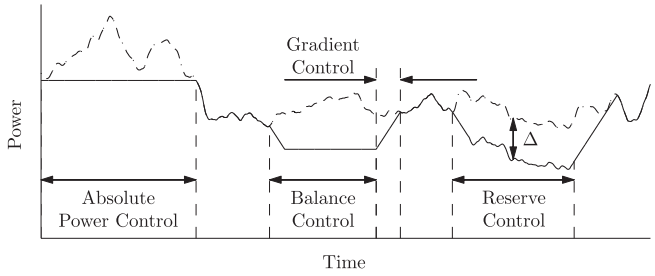

Fig. 2. Some possible operating modes with active power control.

2.2. Dynamic model of the wind turbine

Wind turbines are complex and highly coupled nonlinear dynamical systems. The dominant dynamics lie in the mechanical subsystem, so wind turbines can be modeled as flexible structures undergoing exogenous forces from the airflow and generators. There exist high order models (like FAST, Bladed and others) that describe quite well their behaviour. These models are very useful for many purposes but are not generally used at the control design stage because of their complexity. Instead, low order models capturing the main dynamics are usually used. Since this paper deals with the APC by means of collective pitch and torque control, a model describing the drive-train dynamics suffices for controller design. Later, the controller performance will be assessed using a more complex and complete model.

As widely used in the literature, a third order model capturing the first vibration mode of the drive train is considered. This model is completed with the main dynamics of the pitch actuator:

$$\dot{\Phi} = \Omega_r - \Omega_g/N_g,$$

$$J_r\dot{\Omega}_r = T_r - T_{sh},$$

$$J_g\dot{\Omega}_g = T_{sh}/N_g - T_g,$$

$$\dot{\beta} = -\frac{1}{\tau}\beta + \frac{1}{\tau}\beta_r,$$

where Ω_g is the generator speed, J_r and J_g are the inertia of the rotor and generator, respectively, N_g is the gear box ratio, $T_{sh} = K_s\Phi + B_s\Omega_r - B_s\Omega_g/N_g$ is the shaft torque, K_s the stiffness coefficient, B_s the friction, τ is the time constant of the pitch actuator and β_r the pitch angle command.

The power P_r captured by a wind rotor of radius R facing an airflow of effective speed V and density ρ is

$$P_r = 0.5\pi R^2 \rho C_p(\lambda,\beta)V^3, \tag{1}$$

where C_p describes the turbine aerodynamics. This power coefficient is a nonlinear function of the pitch angle β and the tip-speed-ratio $\lambda = R\Omega_r/V$. This coefficient takes its maximum $C_{p\max}$ at (λ_o,β_o).

The torque T_r that the airflow develops on the rotor is

$$T_r(V,\beta,\Omega_r) = P_r(V,\beta,\Omega_r)/\Omega_r. \tag{2}$$

For controller design, the highly nonlinear T_r is usually linearized along the operating trajectory:

$$\widehat{T}_r = B_r(t)\widehat{\Omega}_r + k_V(t)\widehat{V} + k_\beta(t)\widehat{\beta}, \tag{3}$$

where

$$B_r(t) = \left.\frac{\partial T_r}{\partial \Omega_r}\right|_{\mathrm{op}(t)}, k_V(t) = \left.\frac{\partial T_r}{\partial V}\right|_{\mathrm{op}(t)}, k_\beta(t) = \left.\frac{\partial T_r}{\partial \beta}\right|_{\mathrm{op}(t)}.$$

The hat over the variables denote deviations w.r.t. the point $\mathrm{op}(t) = \{V(t),\beta(t),\Omega_r(t)\}$ where the turbine operates at time t. It should be noted that the conventional operating locus can be parameterized by wind speed since both pitch and rotational speed are uniquely determined by wind speed along A–N–M. The gains B_r, k_V and k_β as function of V for the conventional operating locus are drawn with thick trace in Fig. 3. When the operating region of the wind turbine is extended to achieve APC, different functions of V arise for each power demand as can be seen in Fig. 3. In the figure, the power demand is normalized w.r.t. the rated power, i.e. $P_{pu} = \frac{P_d}{P_N}$.

The following time-varying linear model describes the local dynamics around the operating trajectory (op(t)):

$$\dot{x} = \begin{bmatrix} 0 & 1 & -1/N_g & 0 \\ -K_s/J_r & (B_r - B_s)/J_r & B_s/J_r & k_\beta/J_r \\ K_s/J_gN_g & B_s/J_gN_g & -B_s/J_gN_g^2 & 0 \\ 0 & 0 & 0 & -1/\tau \end{bmatrix} x + \begin{bmatrix} 0 & 0 & 0 \\ k_V/J_r & 0 & 0 \\ 0 & -1/J_g & 0 \\ 0 & 0 & 1/\tau \end{bmatrix} \begin{bmatrix} \widehat{V} \\ u \end{bmatrix}, \tag{4}$$

where $x = \left[\widehat{\Phi}\ \widehat{\Omega}_r\ \widehat{\Omega}_g\ \widehat{\beta}\right]^T$ is the state, $u = [T_g\ \beta_r]^T$ the control input and $\widehat{V}$ the wind speed disturbance. On the extended operating region for APC, this time-varying model can be parameterized in terms of wind speed and power demand according to Fig. 3.

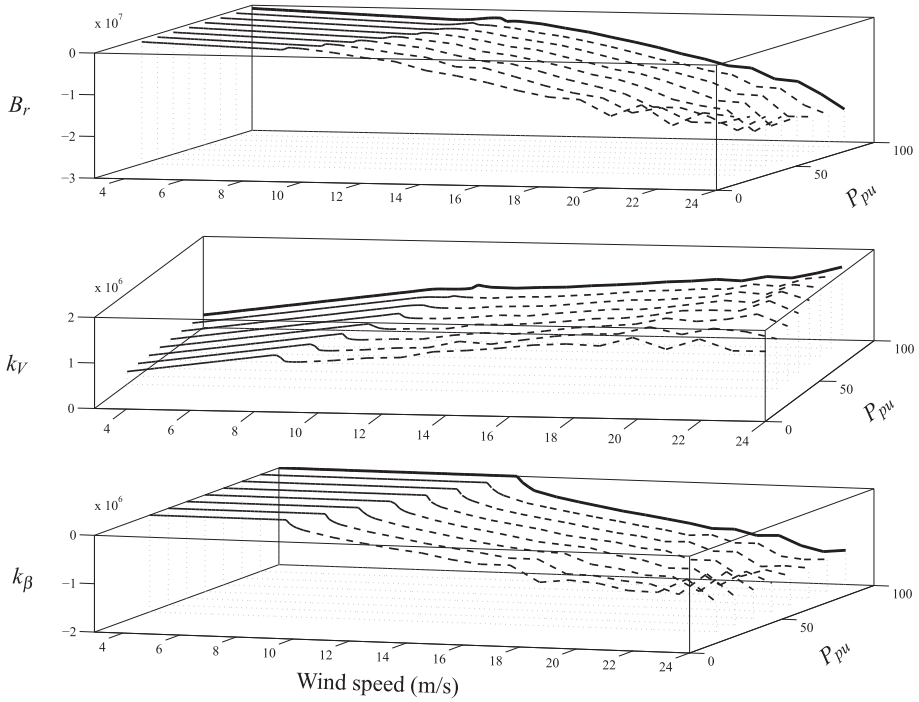

Fig. 3. Linearization coefficient values B_r, k_V and k_β for the whole operating range.

3. Control design

3.1. Control topology

Fig. 4 sketches the two-loop control topology considered in this paper. The rotational speed is controlled by means of the generator torque under partial load conditions and by means of the pitch angle and generator torque under full load operation. The generator torque effectively applied to the wind turbine is built as function of the rotational speed. The L.U.T. constructs the traditional static torque-speed curve for maximum energy capture (1) as in commercial wind turbine control systems, whereas the min(,) function assures that the capture power does not exceed the power demand. In high wind speeds, the pitch controller regulates the rotational speed at its rated value Ω_N. Because of actuator saturation, this controller is only active in region 3e. Therefore, as usual, AW compensation is incorporated to the control system so as to avoid undesirable behaviour in the transition region 2e.

3.2. LPV model for gain-scheduled pitch control design

The first step to design an LPV controller is to find a suitable LPV description of the nonlinear model. The basis for this LPV description is the time-varying model (4) parameterized by V and P_{pu} on the extended operating region. We take advantage here of the decoupled control topology and the fact that only the pitch controller is gain scheduled. The pitch controller is only active in region 3e where a one-to-one relationship exists among V and β for each power demand. So, instead of parameterizing the dynamic model in terms of V and P_{pu}, it can be parameterized in terms of β and P_{pu}. In this way, both parameters are known. As a result, the parameter vector θ and the region Θ where it lives can be defined as

$$\begin{aligned} \theta &= \begin{bmatrix} \beta & P_{pu} \end{bmatrix}^T \\ \Theta &= \{[\beta_0 \;\; \beta_{\max}], [0 \;\; 1]\} \end{aligned} \tag{5}$$

From (4) and (5), the LPV description of the two-mass model discussed in Section 2.2 is

$$G(\theta): \begin{cases} \dot{x}(t) = A(\theta)x(t) + Bu(t), \\ y(t) = Cx(t), \end{cases} \tag{6}$$

where B and C are constant matrices and $A(\theta)$ is affine in B_r and k_β, i.e.

$$A(\theta) = \sum_{j=0}^{2} f_j(\theta)A_j; f_0(\theta) = 1; f_1(\theta) = B_r(\theta); f_2(\theta) = k_\beta(\theta),$$

being the constant matrices

$$A_0 = \begin{bmatrix} 0 & 1 & -1/N_g & 0 \\ -K_s/J_r & -B_s/J_r & -B_s/J_r N_g & 0 \\ K_s/N_g J_g & -B_s/N_g J_g & -B_s/J_g N_g^2 & 0 \\ 0 & 0 & 0 & -1/\tau \end{bmatrix}$$

$$A_1 = \begin{bmatrix} 0 & 0 & 0 & 0 \\ 0 & -1/J_r & 0 & 0 \\ 0 & 0 & 0 & 0 \\ 0 & 0 & 0 & 0 \end{bmatrix} \quad A_2 = \begin{bmatrix} 0 & 0 & 0 & 0 \\ 0 & 0 & 0 & 1/J_r \\ 0 & 0 & 0 & 0 \\ 0 & 0 & 0 & 0 \end{bmatrix},$$

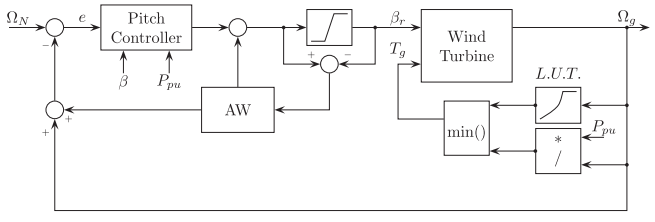

Fig. 4. Proposed control scheme.

$$B_j = [B_{10} \quad B_{20}] = \begin{bmatrix} 0 & 0 \\ 0 & 0 \\ -1/Jg & 0 \\ 0 & 1/\tau \end{bmatrix}, B_{1j} = B_{2j} = 0, j = 1,2$$

$$C_0 = [0 \quad 0 \quad 1 \quad 0], C_1 = C_2 = 0.$$

Note that the term associated to the wind speed (*i.e.*, k_V) in (4) is not included in (6) since it does not affect stability.

Fig. 5 shows the pitch controller LPV parametrization on the operating region 3e.

4. LPV controller synthesis

Fig. 6 shows the setup for LPV pitch controller design. Following the guidelines in Refs. [11,21], the LPV augmented plant can be described as:

$$\begin{bmatrix} \dot{x}_{ap}(t) \\ z(t) \\ y(t) \end{bmatrix} = \begin{bmatrix} A_{ap}(\theta(t)) & B_w(\theta(t)) & B_u(\theta(t)) \\ C_z(\theta(t)) & D_{zw}(\theta(t)) & D_{zu}(\theta(t)) \\ C_y(\theta(t)) & 0 & 0 \end{bmatrix} \begin{bmatrix} x_{ap}(t) \\ w(t) \\ u(t) \end{bmatrix} \quad (7)$$

with $x \in \mathbb{R}^{n_s}$ being the state, $z \in \mathbb{R}^{n_z}$ the performance output, $y \in \mathbb{R}^{n_y}$ the measured variable, $w \in \mathbb{R}^{n_w}$ the disturbance and $u \in \mathbb{R}^{n_u}$ the control action. The parameter $\theta \in \mathbb{R}^{n_p}$ lies in a compact set Θ. This model is affine in the same continuous functions f_j ($j = 1,\ldots,2$) as the LPV wind turbine model (6).

The synthesis problem consists in finding a stabilizing LPV gain-scheduled controller

$$\begin{bmatrix} \dot{x}_c(t) \\ u(t) \end{bmatrix} = \sum_{j=0}^{2} f_j(\theta(t)) \begin{bmatrix} A_{c,j} & B_{c,j} \\ C_{c,j} & D_{c,j} \end{bmatrix} \begin{bmatrix} x_c(t) \\ e(t) \end{bmatrix}, \quad (8)$$

so that the performance constraint

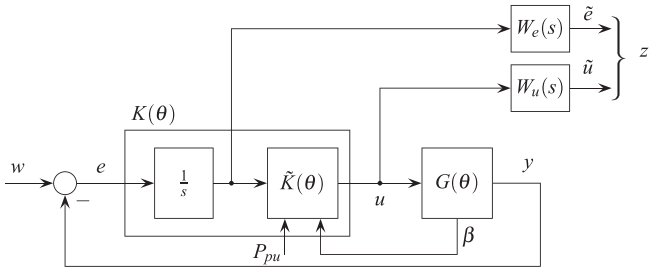

Fig. 6. Setup for the design of the LPV pitch controller.

$$||T_{zw}||_{\mathscr{L}_2} = \sup_{\substack{w \neq 0 \\ \theta \in \Theta}} \frac{||z||_2}{||w||_2} < \gamma \quad (9)$$

is fulfilled, where $||z||_2 = \int z^T z dt$ and $\gamma > 0$ [22]. In this way, the design of the LPV gain-scheduling controller (8) is similar to H_∞ optimal control, *i.e.*, the control specifications are expressed as the minimization of the induced $\mathscr{L}_2$ norm of the operator T_{zw}:$w \rightarrow z$, mapping the disturbance w to the output z. Consequently, before designing an LPV controller, it is necessary to define the performance signal z, the disturbance w and the interconnection between the plant and controller.

The design can be stated as a mixed sensitivity problem where a compromise between rotational speed deviations and pitch activity needs to be fulfilled. Therefore, the disturbance w is the rotational speed set-point and the performance signal is given by $z = [\tilde{e} \quad \tilde{u}]^T$, where

$$\tilde{e} = W_e(\Omega_N - \Omega_g), \tilde{u} = W_u u.$$

The weighting functions W_e and W_u penalize the speed error in low frequencies and the high frequency components of the control

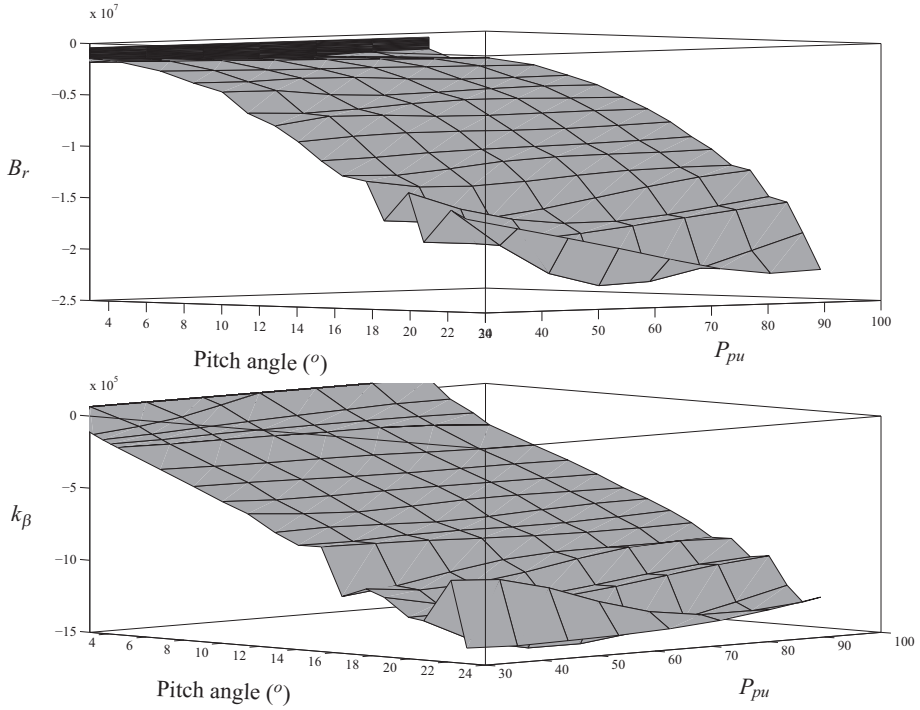

Fig. 5. LPV parametrization in the pitch controller operating region.

action, respectively. Since it appears in the same way as the additive uncertainty, W_u allows covering also the model uncertainty. Integral action is included to ensure zero steady-state error. For stabilizability reasons, the controller is factorized as $K(\theta) = (1/s)\cdot\tilde{K}(\theta)$ [23].

This controller is computed by solving the following optimization problem with LMIs constraints.

$$\begin{bmatrix} XA_{ap}(\theta)+\widehat{B}_c(\theta)C_y+(\star) & \star & \star & \star \\ \widehat{A}_c(\theta)^T+A_{ap}(\theta)+B_uD_c(\theta)C_y & A_c(\theta)Y+B_u\widehat{C}_c(\theta)+(\star) & \star & \star \\ \left(XB_w(\theta)+\widehat{B}_c(\theta)D_{zu}\right)^T & B_w(\theta)^T & -\gamma I_{n_w} & \star \\ C_z(\theta)+D_{zu}D_c(\theta)C_y & C_z(\theta)Y+D_{zu}\widehat{C}_c(\theta) & D_{zw}(\theta) & -\gamma I_{n_z} \end{bmatrix} < 0. \tag{10}$$

minimize $\gamma(X, Y, \widehat{A}_c(\theta), \widehat{B}_c(\theta), \widehat{C}_c(\theta), D_c(\theta))$,
subject to (10) and

$$\begin{bmatrix} X & I \\ I & Y \end{bmatrix} > 0, X = X^T > 0, Y = Y^T > 0,$$

for all $\theta \in \Theta$ and with

$$\widehat{A}_c(\theta) = \sum_{j=0}^{m} f_j(\theta(t))\widehat{A}_{c,j}, \widehat{B}_c(\theta) = \sum_{j=0}^{m} f_j(\theta(t))\widehat{B}_{c,j},$$

$$\widehat{C}_c(\theta) = \sum_{j=0}^{m} f_j(\theta(t))\widehat{C}_{c,j}, \widehat{D}_c(\theta) = \sum_{j=0}^{m} f_j(\theta(t))\widehat{D}_{c,j}.$$

The controller matrices are given by

$$A_c(\theta) = N^{-1}\left(\widehat{A}_c(\theta) - X\left(A(\theta) - B_uD_c(\theta)C_y\right)Y - \widehat{B}_c(\theta)C_yY - XB_u\widehat{C}_c(\theta)\right)M^{-T},$$

$$B_c(\theta) = N^{-1}\left(\widehat{B}_c(\theta) - XB_uD_c(\theta)\right),$$

$$C_c(\theta) = \left(\widehat{C}_c(\theta) - D_c(\theta)C_yY\right)M^{-T},$$

where $I - XY = NM^T$ [11]. This is a convex optimization problem with infinite number of constraints. To reduce the problem to a finite number of LMIs, the parameter space $\Theta = \{[\beta_0\ \beta_{max}],[0\ 1]\}$ is sampled at a set of points $\Theta_g = \{\theta_l, l = 1,\ldots,n_p\}$. Then, the constraint (10) is evaluated at every point in the grid. If the grid is dense enough, then the solution is a good approximation to the infinite dimensional problem.

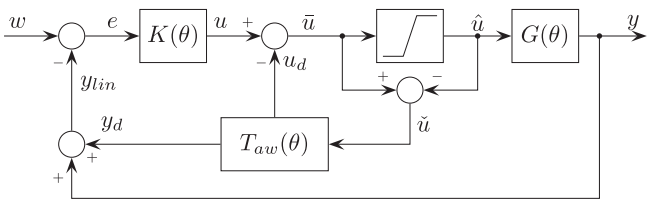

Fig. 7. Anti-windup compensation scheme.

4.1. AW compensation

The AW compensation scheme proposed in this paper is similar to the one in Ref. [24], but now designed for a wider region. The scheme proposed in this paper is inspired on the theoretical framework introduced in Ref. [25] and sketched in Fig. 7. The AW compensation proposed here comprises two compensation terms: one (u_d) acting on the controller output u and the other y_d on the controller input e. Defining

$$\begin{bmatrix} u_d(t) \\ y_d(t) \end{bmatrix} = T_{aw}(\theta(t)) * \check{u}(t) = \begin{bmatrix} U(\theta(t)) - I \\ V(\theta(t)) \end{bmatrix} * \check{u}(t),$$

where $V(\theta) = G(\theta)\cdot U(\theta)$ and * denotes the input-output mapping, it can be proved after some system manipulations that the compensation scheme in Fig. 7 is equivalent to the block diagram of Fig. 8. It can be inferred from this figure that $U(\theta)$ must be designed to ensure stability of the closed loop comprising $U(\theta) - I$ and the nonlinear operator, as well as to minimize the effect of y_d on the controlled variable. Moreover, factorizing the LPV system $G(\theta)$ in coprime factors [26], the AW compensator design comes down to the design of a parameter varying state feedback gain fulfilling an induced $\mathscr{L}_2$ norm condition. More precisely, let

$$\begin{bmatrix} \dot{x}_{aw}(t) \\ u_d(t) \\ y_d(t) \end{bmatrix} = \sum_{j=0}^{2} f_j(\theta) \begin{bmatrix} A_j + B_2H_j & B_j \\ H_j & 0 \\ C_j & 0 \end{bmatrix} \begin{bmatrix} x_{aw}(t) \\ \check{u}(t) \end{bmatrix}$$

be the state-space realization of $T_{aw}(\theta)$, where $H(\theta) = \sum_{j=0}^{2} f_j(\theta)H_j$ is a state-feedback gain such that $T_{aw}(\theta)$ is quadratically stable for $\theta \in \Theta$. Then, using the Small Gain Theorem, the AW compensator will ensure quadratic stability during saturation if $\|U(\theta) - I\|_{\mathscr{L}_2} < 1$. The minimization of the effect on the controlled variable can similarly be expressed as $\|V(\theta)\|_{\mathscr{L}_2} < \nu$. Both conditions will be satisfied if

$$\left\| \begin{matrix} U(\theta) - I \\ V(\theta) \end{matrix} \right\|_{\mathscr{L}_2} < \nu, \tag{12}$$

with $\nu < 1$. Therefore, using standard results of LPV theory [22,27], the design of the AW compensation consists in solving the following optimization procedure.

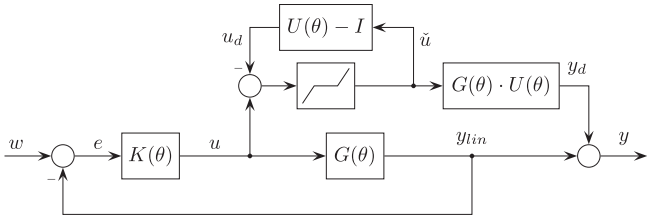

Fig. 8. Equivalent representation of the AW compensation scheme in Fig. 7.

minimize $\nu(Q,W(\theta))$,
subject to

$$\begin{bmatrix} QA(\theta)+B_{20}W(\theta)+(\star) & \star & \star & \star \\ B_{20}^T & -\nu I_{n_u} & \star & \star \\ W(\theta) & 0 & -\nu I_{n_u} & \star \\ C_0 Q & 0 & 0 & -\nu I_{n_y} \end{bmatrix} < 0,$$

$$Q = Q^T > 0, \nu < 1.$$

for all $\theta \in \Theta$ with $\star$ induced by symmetry and $W(\theta) = \sum_{j=0}^{2} f_j(\theta) W_j$. The state feedback is then computed as $H(\theta) = Q^{-1}W(\theta)$. Like in the LPV controller design, the parameter space Θ is sampled at a set of points $\theta \in \Theta_g$.

Note that the AW compensation only depends on the non saturated system $G(\theta)$.

4.2. Unified LPV controller

Since both the pitch controller and the AW compensation are designed in the same LPV framework, it is possible to merge both controller in a single one. This property provides an easier and compact implementation.

$$\begin{bmatrix} \dot{x}_{c+aw}(t) \\ u(t) \end{bmatrix} = \sum_{j=0}^{2} f_j(\theta) \begin{bmatrix} \overline{A}_{c,j} & \overline{B}_{c1,j} & \overline{B}_{c2,j} \\ \overline{C}_{c,j} & D_{c,j} & 0 \end{bmatrix} \begin{bmatrix} x_{c+aw}(t) \\ e(t) \\ \check{u}(t) \end{bmatrix}, \quad (13)$$

$$\overline{A}_{c,j} = \begin{bmatrix} A_{c,j} & -B_{c,j}C_2 \\ 0 & A_j + B_2 H_j \end{bmatrix}, \overline{B}_{c1,j} = \begin{bmatrix} B_{c,j} \\ 0 \end{bmatrix},$$

$$\overline{B}_{c2,0} = \begin{bmatrix} 0 \\ B_j \end{bmatrix}, \overline{C}_{c,j} = \begin{bmatrix} C_{c,j} & -(D_{c,j}C_2 + H_j) \end{bmatrix}.$$

where the parameter dependence of the main controller is preserved.

4.3. Controller tuning

Once the disturbance and performance outputs are selected in the controller setup, the controller tuning essentially consists in choosing the performance weights W_e and W_u. For the 5 MW FAST wind turbine benchmark, we select:

$$W_e(s) = 2.5, W_u(s) = 0.015 \frac{s/3.5 + 1}{s/350 + 1}.$$

This choice, where W_e implicitly includes the integral action of the controller, ensures good rotational speed regulation with zero steady state error by means of low pitch activity. W_u also provides some degree of robustness with respect to unmodeled dynamics, particularly at high frequencies.

The optimization problems to obtain the LPV controller and the anti-windup compensator were solved with Sedumi [28] and YALMIP [29]. To this end, the parameter space Θ was gridded in 120 points, 15 in the range 0–30° (β) and 8 in the range 30–100% (P_{pu}).

5. Simulation results

The control proposal was assessed on the 5 MW FAST wind turbine benchmark [19] under the Matlab/Simulink/FAST environment [30]. The following DOFs were enabled: FlapDOF1, FlapDOF2, EdgeDOF, DrTrDOF, GenDOF, YawDOF, TwFADOF1, TwFADOF2, TwSSDOF1, TwSSDOF2, CompAero. For comparative purposes, gain

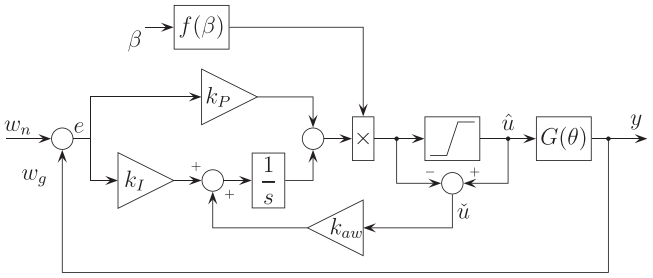

Fig. 9. PI control configuration.

scheduled PI and $\mathscr{H}_\infty$ strategies were also evaluated [19,31–33]. In both cases, the same $\min(\cdot,\cdot)$ control torque law as in the LPV case was used.

The gain-scheduled PI controller, in combination with the benchmark wind turbine under analysis, is broadly used to assess the performance of new control strategies. It was designed following the guidelines in Refs. [19,31]. Basically, the PI controller was tuned as in Ref. [19] after linearizing the wind turbine model at the operating point $(\overline{V}, \overline{\beta}, \overline{\Omega_r}) = (11.4\text{m/s}, 0, 12.1\text{rpm})$. The controller gains were calculated to achieve appropriate damping (0.7) and natural frequency (0.6 rad/s) [31]. As the controller ensures the desired behaviour only at the design operating point, a pitch-dependent gain is applied to compensate for the nonlinear rotor torque. This gain is function of β obtained by fitting the values of k_β along the operating locus. In addition, a classical anti-windup compensation was added to improve the transient between regions 1 and 3. The PI tuning constants are $K_P(\beta = 0) = 0.01882681$ s, $K_I(\beta = 0) = 0.008068634$. The function that makes the gain scheduling is $f(\beta) = 1/(1 + \beta/\beta_k)$, where $\beta_k = 6.30236$ is the blade pitch angle at double rotor power. Fig. 9 shows the PI control topology.

The $\mathscr{H}_\infty$ pitch controller was designed according to the control setup in Fig. 10. The same gain scheduling $f(\beta)$ as before is included to compensate for the nonlinearity of k_β. Other nonlinearities along classical region 3 are covered with additive uncertainty W_Δ depicted in Fig. 11. The speed error and control effort are weighted by

$$W_e'(s) = M(s)W_e(s) = \frac{1}{s}k_e, \quad W_u = k_u \frac{s/0.1\omega_u + 1}{s/\omega_u + 1}$$

with $k_e = 0.3$, $\omega_u = 50$ and $k_u = 0.25$. The frequency response of these weight functions are also shown in Fig. 11. The weight W_u' that appears in Fig. 10 must be the more demanding between W_u and W_Δ at every frequency. In this case $W_u' = W_u$ suffices. The ∞-norm of the closed loop transfer function T_{zw} resulted in 0.977. In particular, the norm of the transfer function from Ω_N to the control signal β, *i.e.*,

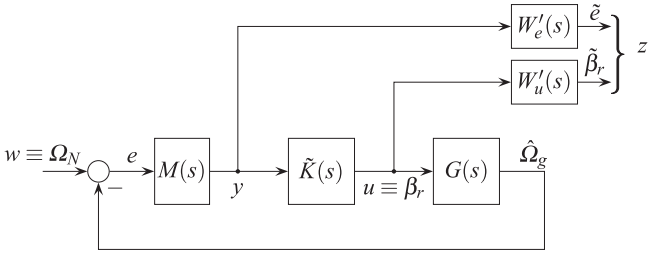

Fig. 10. $\mathscr{H}_\infty$ control configuration.

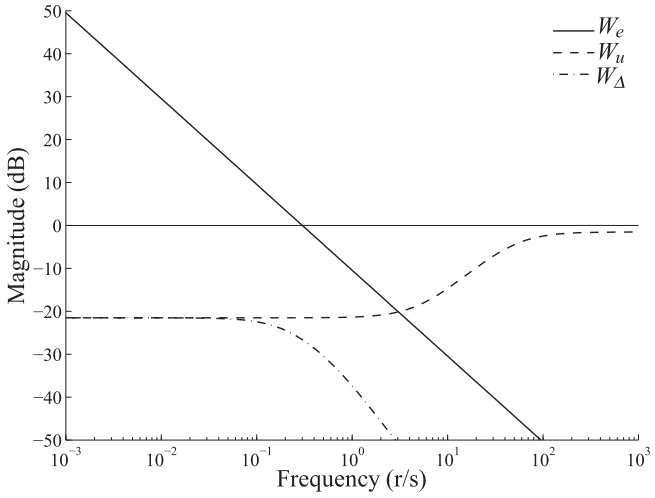

Fig. 11. Weights functions used in the $\mathscr{H}_\infty$ pitch control design.

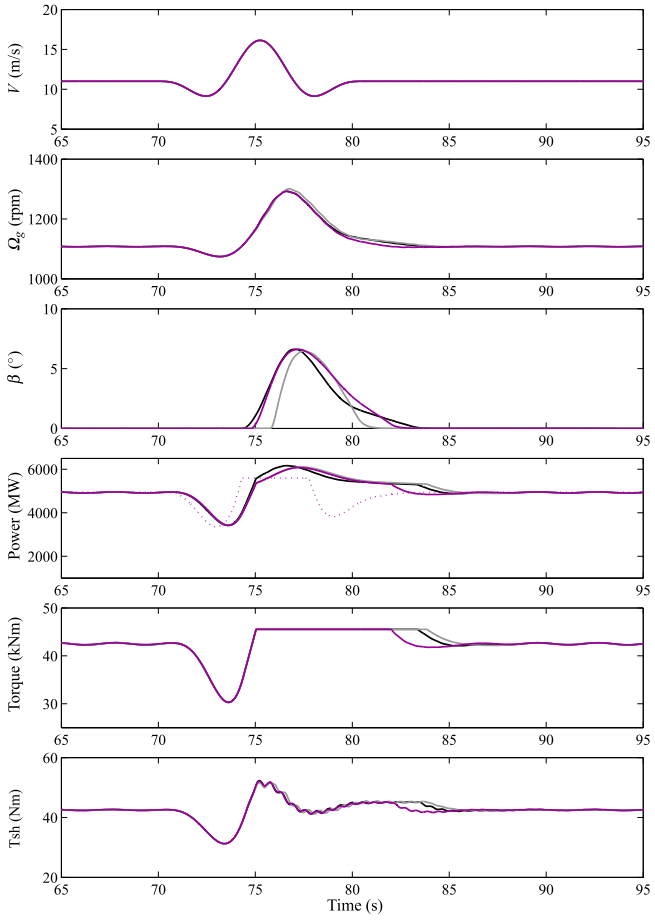

Fig. 12. System response to a wind gust profile with rated power demand. Black lines: LPV controller, grey lines: PI controller, purple lines: $\mathscr{H}_\infty$ controller, dotted-line: instantaneous maximum power saturated to rated value. (For interpretation of the references to color in this figure legend, the reader is referred to the web version of this article.)

$$\left\| K(I+KG)^{-1} \right\|_\infty = 0.972.$$

Since the norm is lower than 1, stability against covered modelling errors is guaranteed. For the AW compensation, the same approach as in the LPV case was used, but now LTI.

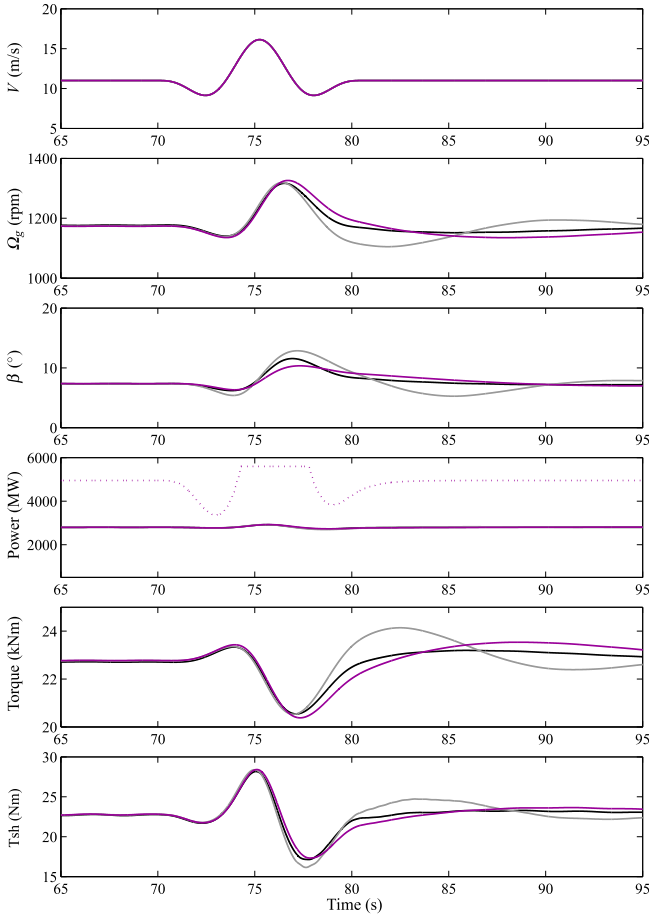

Fig. 13. System response to a wind gust profile with 50% rated power demand. Black lines: LPV controller, grey lines: PI controller, purple lines: $\mathscr{H}_\infty$ controller, dotted-line: instantaneous maximum power saturated to rated value. (For interpretation of the references to color in this figure legend, the reader is referred to the web version of this article.)

Four scenarios were simulated. In the first scenario, Fig. 12 and 13, a wind gust in the transition region for two different power set points were considered. Fig. 12 shows the response when APC is inactive, i.e. when the power demand equals the rated power. Although the LPV controller exhibits a slightly better speed regulation than the PI and the $\mathscr{H}_\infty$, the responses are quite similar putting in evidence that these controllers are properly tuned for the classical operating curve. Fig. 13 shows the response to the same wind gust for a 50% rated power demand. This case shows the mistuning of the PI and $\mathscr{H}_\infty$ controllers outside their design operating region that can be appreciated both in the speed regulation and pitch action. In fact, poorly damped oscillations appear in all variables of interest.

The second scenario, Fig. 14, corresponds to a wind rise growing from 6 m/s to 15 m/s in 10 s. In this case, an external set-point of 50% rated power is settled. The output power response of all controllers are very similar since they apply the same control law. However, significant differences appear in the other variables putting in evidence the superior performance of the proposed controller. For instance, the LPV control approaches rated speed smoothly without overshoot whereas the PI and $\mathscr{H}_\infty$ controls leads to a large overshoot. This much better speed regulation feature is achieved with a smooth pitch control action. This lower pitch

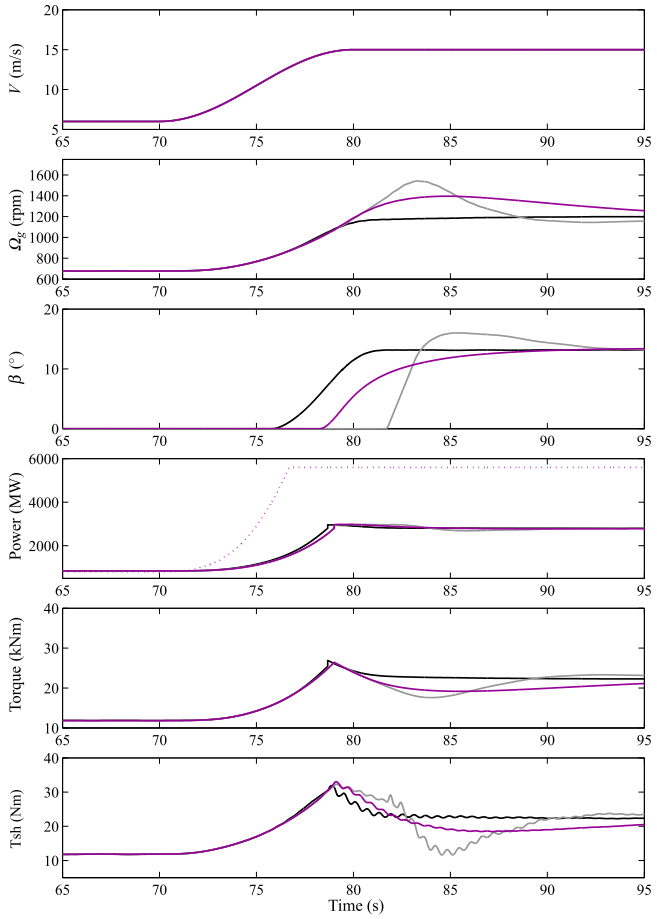

Fig. 14. System response to a wind rise profile with 50% rated power demand. Black lines: LPV controller, grey lines: PI controller, purple lines: $\mathscr{H}_\infty$ controller, dotted-line: instantaneous maximum power saturated to rated value. (For interpretation of the references to color in this figure legend, the reader is referred to the web version of this article.)

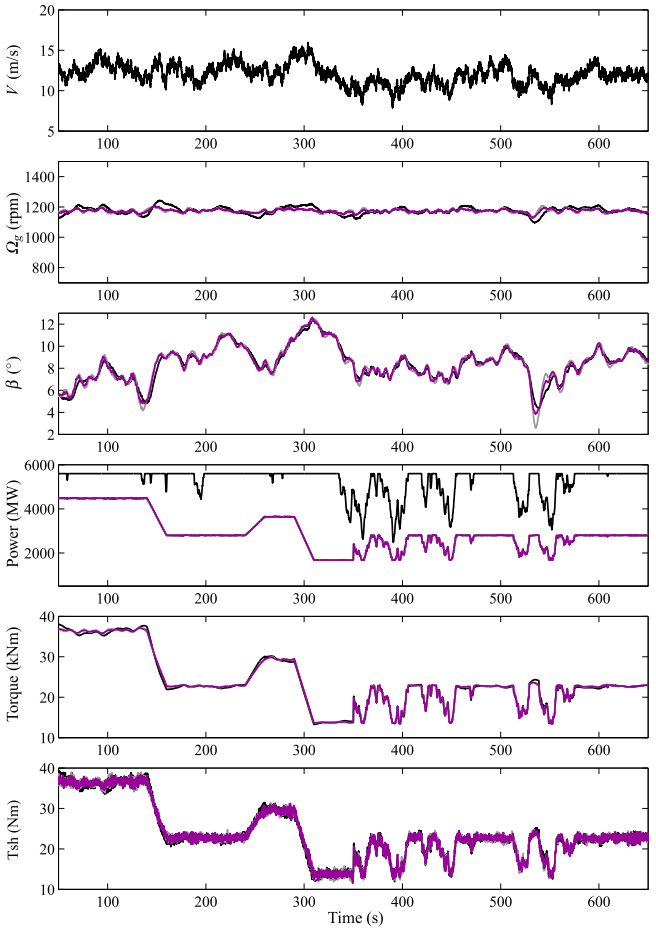

Fig. 15. System response to a realistic wind profile with different external references: constant power generation, limited rated power change and generation with reserve. Black lines: LPV controller, grey lines: PI controller, purple lines: $\mathscr{H}_\infty$ controller, dotted-line: instantaneous maximum power saturated to rated value. (For interpretation of the references to color in this figure legend, the reader is referred to the web version of this article.)

activity, in turn, contributes to less mechanical loads extending the wind turbine lifetime.

In the third scenario, Fig. 15, a 10 min long realistic wind profile was simulated. The wind profile was generated with Turbsim [34]. In this case, three types of control modes can be seen. During the first 5 min, a sequence of different power set-points are followed subject to gradient limitation. During the last 5 min, 50% power reserve is demanded. By simple inspection, it can be seen that the LPV controller causes less high frequency pitch activity and less high frequency speed oscillations.

5.1. Load analysis

Although no representative variables of mechanical loads are fed back nor taken into account in the design process, the lower pitch activity achieved with the selected weight functions of the LPV controller carries a load reduction both in the shaft and the blades. This load reduction can be checked using the post-processor MExtremes written by the NWTC (National Wind Technology Center) at the NREL (National Renewable Energy Laboratory).

Table 1 is an extreme event table with their values taken from the extreme event tables generated with MExtremes for all three controllers. The FAST outputs of the previous simulations (Figs. 12–15) were used to get the values. For each controller, an extra column with the difference between the maximum and minimum values was included. With the aim of showing a comparative figure, two extra comparative columns using LPV as baseline controller were added. These columns were colored with the following rule: green: decrease of 10% or more w.r.t. LPV; red: increase of 10% or more w.r.t. LPV; yellow: in between of the previous cases (nor increase or decrease is considered). Table 2 contains a description of the parameters in Table 1.

As can be seen, the LPV controller exhibits much better time response than the PI and $\mathscr{H}_\infty$. In fact, less settling time and overshoots are observed in the controlled speed, torque and pitch action. Additionally, while similar extreme loads are obtained with the $\mathscr{H}_\infty$ controller, the LPV one significantly improves the extreme loads in comparison with the PI controller.

5.2. Loss of grid case

The fourth and last scenario is aimed to show the controller behaviour under a critical situation. Particularly the resistant torque is set zero at $t = 69$ [s] simulating a grid loss (as can be done with the command TimGenOf in the FAST environment). The idea behind this scenario is to show that the LPV controller can make a fast scheduling like other techniques. This scenario is performed under an extreme wind gust with the objective of adding a more demand case. The results are presented in Fig. 16. As can be seen,

Table 1
Extreme event analysis.

			LPV		PI		Hinf			
Parameter	Type	Unit	Calculated Extreme	Diff	Calculated Extreme	Diff	Calculated Extreme	Diff	PI %	Hinf %
OoPDefl1	Minimum	m	-0.31	7.80	-1.24	9.12	-0.11	7.80	14.40	-0.01
OoPDefl1	Maximum	m	7.49		7.87		7.69			
IPDefl1	Minimum	m	-1.38	1.87	-1.38	2.06	-1.33	1.81	9.27	-3.21
IPDefl1	Maximum	m	0.50		0.68		0.48			
OoPDefl2	Minimum	m	-0.05	7.10	-1.13	8.87	0.13	7.09	19.91	-0.19
OoPDefl2	Maximum	m	7.06		7.74		7.22			
IPDefl2	Minimum	m	-1.33	1.82	-1.31	1.78	-1.29	1.80	-2.26	-1.26
IPDefl2	Maximum	m	0.49		0.47		0.50			
OoPDefl3	Minimum	m	-0.42	7.75	-0.79	8.89	0.01	7.58	12.89	-2.22
OoPDefl3	Maximum	m	7.33		8.10		7.59			
IPDefl3	Minimum	m	-1.48	2.00	-1.47	1.88	-1.49	1.94	-6.28	-3.06
IPDefl3	Maximum	m	0.52		0.41		0.46			
RootFxc2	Minimum	kN	14.51	371.59	-46.76	451.76	23.91	367.89	17.75	-1.00
RootFxc2	Maximum	kN	386.10		405.00		391.80			
RootFyc2	Minimum	kN	-224.20	395.70	-226.80	402.10	-223.60	396.30	1.59	0.15
RootFyc2	Maximum	kN	171.50		175.30		172.70			
RootFzc2	Minimum	kN	32.12	837.78	32.19	827.71	32.22	827.48	-1.22	-1.24
RootFzc2	Maximum	kN	869.90		859.90		859.70			
RootMxc2	Minimum	kN m	-3546.04	8609.04	-3637.00	8843.00	-3579.00	8650.00	2.65	0.47
RootMxc2	Maximum	kN m	5063.00		5206.00		5071.00			
RootMyc2	Minimum	kN m	-33.90	13433.90	-2172.00	16572.00	376.00	13294.00	18.94	-1.05
RootMyc2	Maximum	kN m	13400.00		14400.00		13670.00			
RootMzc2	Minimum	kN m	-94.18	241.60	-93.78	245.28	-94.75	247.76	1.50	2.49
RootMzc2	Maximum	kN m	147.42		151.50		153.00			
RotThrust	Minimum	kN	-71.57	1243.57	-176.60	1386.60	-13.55	1204.55	10.32	-3.24
RotThrust	Maximum	kN	1172.00		1210.00		1191.00			
HSShftTq	Minimum	kN m	11.68	40.61	11.56	40.20	11.54	40.58	-1.02	-0.07
HSShftTq	Maximum	kN m	52.29		51.76		52.12			
LSSGagMya	Minimum	kN m	-4035.00	8064.80	-3730.00	7922.00	-3583.00	7746.33	-1.80	-4.11
LSSGagMya	Maximum	kN m	4029.80		4192.00		4163.33			

Table 2
Parameters for load analysis.

Parameter	Description
$OoPDefl_i$	Blade *i* out-of-plane tip deflection (relative to the pitch axis)
$IPDefl_i$	Blade *i* in-plane tip deflection (relative to the pitch axis)
$RootFxc_i$	Blade *i* out-of-plane shear force at the blade root
$RootFyc_i$	Blade *i* in-plane shear force at the blade root
$RootFzc_i$	Blade *i* axial force at the blade root
$RootMxc_i$	Blade *i* in-plane moment (i.e., the moment caused by in-plane forces) at the blade root
$RootMyc_i$	Blade *i* out-of-plane moment (i.e., the moment caused by out-of-plane forces) at the blade root
$RootMzc_i$	Blade *i* pitching moment at the blade root
RotThrust	LSS thrust force (this is constant along the shaft and is equivalent to the rotor thrust force)
HSShftTq	HSS torque (this is constant along the shaft)
LSSGagMya	Rotating LSS bending moment at the shaft's strain gage (shaft strain gage located by input ShftGagL)

after the failure the blades are pitched to maintain speed at its rated value. Other possible action is setting the reference speed to zero with the aim of slowing down the rotor before applying the brakes. It can be seen in the figure that the LPV controller achieves a suitable response, perhaps even better than the other two cases.

6. Conclusions

When extending the maximum power operating locus to achieve active power control, some challenges arise in the control design. As it was shown by simulation of the FAST wind turbine benchmark, the traditional gain-scheduled pitch PI tuning leads to oscillatory responses for power demands below rated. The controller gains could be modified to improve response at certain power set-points, but performance at rated power regulation would be inevitably deteriorated. The addition of an extra scheduling parameter to the PI is not trivial, whereas its tuning is harder because of the lack of systematic design rules. Other linear control techniques, such as $\mathscr{H}_\infty$ suffers from the same limitations as it was also shown in the simulations results.

The LPV approach showed to be particularly attractive to design a gain-scheduled pitch controller for active power control, including anti-windup features. In fact, the controller design and implementation is very simple, translating the complexity to the

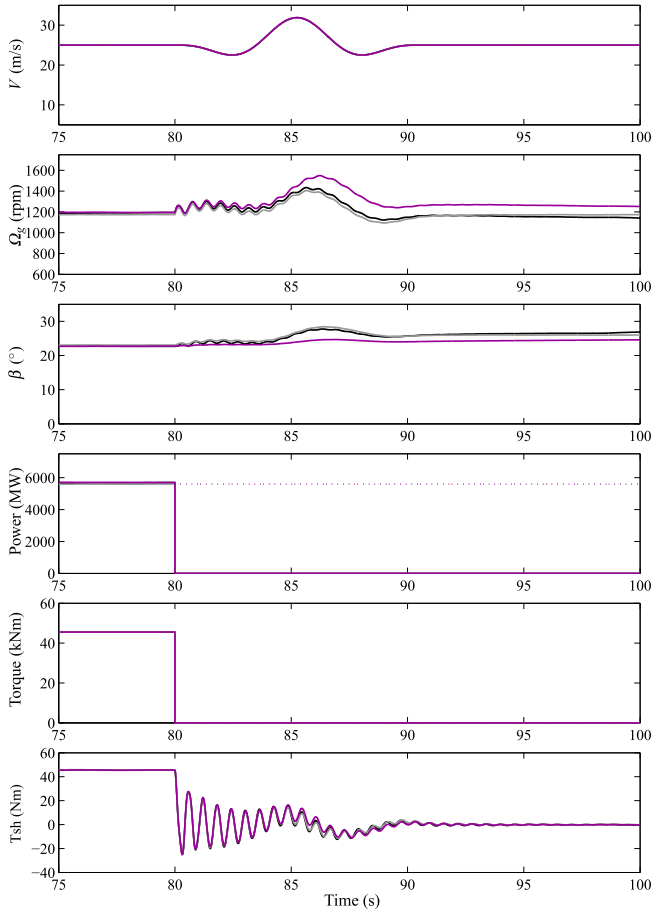

Fig. 16. System response to an extreme wind gust profile with rated power demand and a loss of grid. Black lines: LPV controller, grey lines: PI controller, purple lines: $\mathscr{H}_\infty$ controller, dotted-line: instantaneous maximum power saturated to rated value. (For interpretation of the references to color in this figure legend, the reader is referred to the web version of this article.)

numerical optimization problem. When evaluated on the FAST wind turbine benchmark, the controller developed in this paper exhibits satisfactory performance for different power demands and robustness against the benchmark dynamics not considered during the design procedure. Also, the LPV controller showed a decrease in the aerodynamic loads.

The underlying limitations of ad-hoc gain scheduled linear controllers will be more and more restrictive as new control objectives and controlled variables are incorporated, for instance to mitigate structural loads. Alternatively, the LPV approach seems a friendly framework to design more complex controllers in a systematic way. For instance, structural loads can be considered in the controller design by including them as performance outputs. Furthermore, when available (for instance measuring tower acceleration) they can be included in the feedback loop.

Acknowledgements

This work was supported by Universidad Nacional de La Plata (11/I216), CONICET (PIP0837 2015-2017), CICpba and ANPCyT (PICT 2015-3586) of Argentina.

References

[1] EWEA, Large Scale Integration of Wind Energy in the European Power Supply: Analysis, Issues and Recommendations, EWEA, 2005. Tech. rep.
[2] N. Miller, K. Clark, Advanced controls enable wind plants to provide ancillary services, in: IEEE Power and Energy Society General Meeting, July 2010.
[3] J. Aho, L. Pao, P. Fleming, An active power control system for wind turbines capable of primary and secondary frequency control for supporting grid reliability, in: 51st AIAA Aerospace Sciences Meeting Including the New Horizons Forum and Aerospace Exposition, 2013.
[4] J. Aho, A. Buckspan, J. Laks, P. Fleming, Y. Jeong, F. Dunne, M. Churchfield, L. Pao, K. Johnson, A tutorial of wind turbine control for supporting grid frequency through active power control, in: American Control Conference (ACC), 2012, 2012, pp. 3120–3131, http://dx.doi.org/10.1109/ACC.2012.6315180.
[5] Y. Jeong, K. Johnson, P. Fleming, Comparison and testing of power reserve control strategies for grid-connected wind turbines, Wind Energy 17 (3) (2014) 343–358, http://dx.doi.org/10.1002/we.1578.
[6] F. Pozo, Y. Vidal, L. Acho, N. Luo, M. Zapateiro, Power regulation of wind turbines using torque and pitch control, in: American Control Conference (ACC), 2013, 2013, pp. 6486–6491, http://dx.doi.org/10.1109/ACC.2013.6580856.
[7] H. Ma, B. Chowdhury, Working towards frequency regulation with wind plants: combined control approaches, Renew. Power Gener. IET 4 (4) (2010) 308–316, http://dx.doi.org/10.1049/iet-rpg.2009.0100.
[8] A. Buckspan, J. Aho, P. Fleming, Y. Jeong, L. Pao, Combining droop curve concepts with control systems for wind turbine active power control, in: Power Electronics and Machines in Wind Applications (PEMWA), 2012, IEEE, 2012, pp. 1–8, http://dx.doi.org/10.1109/PEMWA.2012.6316403.
[9] D.J. Leith, W.E. Leithead, Appropriate realization of gain-scheduled controllers with application to wind turbine regulation, Int. J. Control 65 (2) (1996) 223–248, http://dx.doi.org/10.1080/00207179608921695 arXiv.
[10] J.S. Shamma, M. Athans, Guaranteed properties of gain scheduled control for linear parameter-varying plants, Automatica 27 (3) (1991) 559–564, http://dx.doi.org/10.1016/0005-1098(91)90116-J. http://www.sciencedirect.com/science/article/pii/000510989190116J.
[11] P. Apkarian, R.J. Adams, Advanced gain-scheduling techniques for uncertain systems, IEEE Trans. Control Syst. Technol. 6 (1) (1998) 21–32, http://dx.doi.org/10.1109/87.654874.
[12] F.D. Bianchi, R.J. Mantz, C.F. Christiansen, Power regulation in pitch-controlled variable-speed WECS above rated wind speed, Renew. Energ. 29 (11) (2004) 1911–1922.
[13] F.D. Bianchi, R.J. Mantz, C.F. Christiansen, Gain scheduling control of variable-speed wind energy conversion systems using quasi-LPV models, Control Eng. Pract. 13 (2) (2005) 247–255.
[14] F.D. Bianchi, H. De Battista, R.J. Mantz, Wind Turbine Control Systems: Principles, Modelling and Gain Scheduling Design, Advances in Industrial Control, Springer-Verlag London Ltd., London, 2006.
[15] F. Lescher, H. Camblong, O. Curea, R. Briand, LPV control of wind turbines for fatigue loads reduction using intelligent micro sensors, in: Proc. of the American Control Conference, 2007, pp. 6061–6066, http://dx.doi.org/10.1109/ACC.2007.4282790.
[16] K.Z. stegaard, J. Stoustrup, P. Brath, Linear parameter variying control of wind turbines covering both partial load and full load conditions, Int. J. Robust Nonlin. 19 (2008) 92–116.
[17] F. Bianchi, H. De Battista, R. Mantz, Optimal gain-scheduled control of fixed-speed active stall wind turbines, Renew. Power Gener. IET 2 (4) (2008) 228–238, http://dx.doi.org/10.1049/iet-rpg:20070106.
[18] F.D. Bianchi, H. De Battista, R.J. Mantz, Robust multivariable gain-scheduled control of wind turbines for variable power production, Int. J. Syst. Control 1 (2010) 103–112.
[19] J. Jonkman, S. Butterfield, W. Musial, G. Scott, Definition of a 5-MW Reference Wind Turbine for Offshore System Development, NREL, 2009. Technical report.
[20] H. De Battista, R. Mantz, F. Bianchi, Wind Turbines: Types, Economics and Development, Nova, 2011, pp. 277–312. Ch. Control strategies for modern high-power wind turbines.
[21] F. Wu, X.H. Yang, A. Packard, G. Becker, Induced L2-norm control for LPV systems with bounded parameter variation rates, Int. J. Robust Nonlin. 6 (1996) 983–998.
[22] G.S. Becker, A. Packard, Robust performance of linear parametrically varying systems using parametrically-dependent linear feedback, Syst. Control Lett. 23 (3) (1994) 205–215, http://dx.doi.org/10.1016/0167-6911(94)90006-X.
[23] K. Zhou, J. Doyle, K. Glover, Robust and Optimal Control, Prentice Hall, 1996.
[24] F. Inthamoussou, F. Bianchi, H. De Battista, R. Mantz, Lpv wind turbine control with anti-windup features covering the complete wind speed range, Energy Convers. IEEE Trans. 29 (1) (2014) 259–266, http://dx.doi.org/10.1109/TEC.2013.2294212.
[25] M.C. Turner, I. Postlethwaite, A new perspective on static and low order anti-windup synthesis, Int. J. Control 77 (1) (2004) 27–44, http://dx.doi.org/10.1080/00207170310001640116.
[26] W. Xie, T. Eisaka, Design of LPV control systems based on Youla parameterisation, IEE P Contr. Theor. Ap. 151 (4) (2004) 465–472, http://dx.doi.org/10.1049/ip-cta:20040513.
[27] P. Apkarian, P. Gahinet, G. Becker, Self-scheduled H∞ control of linear parameter-varying systems: a design example, Automatica 31 (9) (1995) 1251–1261, http://dx.doi.org/10.1016/0005-1098(95)00038-X.
[28] J. Sturm, Using SeDuMi 1.02, a Matlab toolbox for optimization over symmetric cones, Optim. Method Softw. 11–12 (1999) 625–653.
[29] J. Löfberg, YALMIP: a toolbox for modeling and optimization in MATLAB, in:

Proc. of the CACSD Conference, Taipei, Taiwan, 2004.
[30] NWTC computer-aided engineering tools (FAST by J. Jonkman, Ph.D.), http://wind.nrel.gov/designcodes/simulators/fast/. Last modified 27-February-2013; accessed 26-August-2013.
[31] M. Hansen, A. Hansen, T. Larsen, S. Øye, P. Sørensen, P. Fuglsang, Control Design for a Pitch-regulated, Variable Speed Wind Turbine, RISØ, 2005. Technical report.
[32] F. Bianchi, R. Snchez-Pea, M. Guadayol, Gain scheduled control based on high fidelity local wind turbine models, Renew. Energy 37 (1) (2012) 233–240, http://dx.doi.org/10.1016/j.renene.2011.06.024.
[33] H. Takaai, Y. Chida, K. Sakurai, T. Isobe, Pitch angle control of wind turbine generator using less conservative robust control, in: 2009 IEEE Control Applications, (CCA) Intelligent Control, (ISIC), 2009, pp. 542–547, http://dx.doi.org/10.1109/CCA.2009.5281077.
[34] NWTC computer-aided engineering tools (TurbSim by N. Kelley, B. Jonkman), http://wind.nrel.gov/designcodes/preprocessors/turbsim/. Last modified 30-May-2013; accessed 28-August-2013.